

Koiter asymptotic analysis of folded laminated composite plates

E. J. Barbero

West Virginia University, Morgantown USA

and

A. Madeo, G. Zagari, R. Zinno¹, and G. Zucco

University of Calabria, Arcavacata di Rende, CS, Italy

Abstract

A mixed formulation, four node, flat shell element is proposed for the geometrically nonlinear analysis of laminated composite plates. The element is based on the linear analysis of isotropic folded plates, which is then generalized for nonlinear analysis by using a corotational formulation and Koiter's asymptotic method. Numerical results are presented for buckling and post-critical analysis. The equilibrium paths compare well with those obtained by continuation methods but at a fraction of the computational cost.

Keywords

Laminates, finite element analysis (FEA), computational modeling, numerical analysis.

1 Introduction

Folded laminated composite plates are used in important structures such as pultruded columns in civil infrastructure [1], stiffeners and stiffened panels in aircraft [2], and so on. These structures are susceptible to buckling and their critical and post-critical behavior often controls their design [3].

Stability analysis of laminated composite plates is customarily performed in two stages. First, in what is called buckling analysis, the bifurcation points on the primary path are found by using an eigenvalue analysis. This process is computationally inexpensive. Second, the nonlinear behavior of the imperfect structure is calculated by using a continuation method. This process requires that the analyst chooses an imperfection shape and amplitude, neither of which are usually known for the structure being analyzed. Furthermore, the analysis is incremental and thus computationally expensive. The Riks method is normally used to account for the possibility of snap-through [4].

A computationally less expensive alternative is to use Koiter's asymptotic analysis [5] that provides an effective and accurate strategy for predicting the initial post-critical behavior in both cases of limit or bifurcation points [6–14]. Koiter's analysis yields the bifurcation points and the nonlinear response at a fraction of the cost. Koiter's approach is based on a fourth-order expansion

¹Corresponding author: raffaele DOT zinno AT unical DOT it. The final publication is available at <http://dx.doi.org/10.1016/j.compositesb.2014.01.045>

of the strain energy [15, 16]. So, a careful tuning of both the continuum model and its finite element implementation is needed to obtain accurate results. Specifically, a geometrically exact structural model, at least until the fourth-order, is necessary. This is a very strict requirement [17, 18], but it is important for the accuracy of the approach, which is very sensitive to the correctness of the energy expression.

Koiter's implementations are specific for each plate kinematics. Therefore, a kinematics suitable for the analysis of laminated composites is used in this work, namely first order shear deformation theory (FSDT) [19].

The corotational approach [16], alternatively to total Lagrangian formulation [20], allows us to obtain geometrically exact structural models and fourth-order energy variations of strain energy using an earlier element originally formulated for linear analysis [21] and isotropic folded plates [22].

The linear finite element with corotational framework is called MISS-4 [21]. It is a simple four-node element based on Hellinger-Reissner variational principle. The displacement interpolation is represented by 24 DOFs (3 displacements and 3 rotations per node) while the stress, which is **enforced to be** self equilibrated and isostatic, is represented by 18 parameters. The element matrices are obtained using analytical integration along the contour of the element. The drilling rotations are introduced following Allman's procedure [23, 24] and spurious energy modes are avoided employing an incompatible displacement cubic mode [25].

The effectiveness and accuracy of the proposed nonlinear laminated composite element are then demonstrated for buckling and post-buckling analysis of a standard benchmarks, including a simple supported plate with uniaxial load and several laminate stacking sequences (LSS) [26] and a hinged cylindrical roof [27] displaying strong nonlinear pre-critical behavior. Furthermore, comparison is made with a column with channel cross section, experimentally tested [28], displaying buckling mode interaction, which is particularly difficult to model [29, 30] and crucial for the development of design equations [31].

2 Geometrically linear formulation

Let the initial reference configuration of the element be flat and referred to a local Cartesian frame $\{\mathbf{e}_1, \mathbf{e}_2, \mathbf{e}_3\}$. Let $\{x, y\}$ be the position of the vector along the middle surface Ω lying in the plane defined by the unit vectors $\{\mathbf{e}_1, \mathbf{e}_2\}$; s the thickness along the \mathbf{e}_3 direction, and Γ is the boundary of Ω .

The first-order shear deformable theory (FSDT) is employed [19]. The mixed² Hellinger-Reissner strain energy for a flat shell can be written as

$$\begin{aligned} \Phi[\mathbf{t}, \mathbf{d}] &= \int_{\Omega} \left\{ \mathbf{t}^T \mathbf{D} \mathbf{d} - \frac{1}{2} \mathbf{t}^T \mathbf{E}^{-1} \mathbf{t} \right\} d\Omega \\ \mathbf{t} &= \begin{bmatrix} \mathbf{t}_m \\ \mathbf{t}_f \end{bmatrix}, \quad \mathbf{d} = \begin{bmatrix} \mathbf{d}_m \\ \mathbf{d}_f \end{bmatrix}, \quad \mathbf{D} = \begin{bmatrix} \mathbf{D}_m & \mathbf{0} \\ \mathbf{0} & \mathbf{D}_f \end{bmatrix} \end{aligned} \quad (1)$$

where the vectors \mathbf{t}_m and \mathbf{t}_f are the membrane stress resultants, and the moment and shear resultants, respectively; \mathbf{d}_m and \mathbf{d}_f are the in- and out-plane kinematical parameters, defined as

²Also called hybrid.

follows

$$\mathbf{t}_m = \begin{bmatrix} N_x \\ N_y \\ N_{xy} \end{bmatrix}, \quad \mathbf{t}_f = \begin{bmatrix} M_x \\ M_y \\ M_{xy} \\ S_x \\ S_y \end{bmatrix}, \quad \mathbf{d}_m = \begin{bmatrix} d_x \\ d_y \end{bmatrix}, \quad \mathbf{d}_f = \begin{bmatrix} d_z \\ \varphi_x \\ \varphi_y \end{bmatrix} \quad (2)$$

where N, M, S are the membrane, bending, and shear stress resultants, respectively; d, φ are the midsurface strains and rotations, respectively. The differential operators \mathbf{D}_m and \mathbf{D}_f are defined as

$$\mathbf{D}_m = \begin{bmatrix} \partial/\partial x & 0 \\ 0 & \partial/\partial y \\ \partial/\partial y & \partial/\partial x \end{bmatrix}, \quad \mathbf{D}_f = \begin{bmatrix} 0 & 0 & -\partial/\partial x \\ 0 & \partial/\partial y & 0 \\ 0 & \partial/\partial x & -\partial/\partial y \\ \partial/\partial x & 0 & 1 \\ \partial/\partial y & -1 & 0 \end{bmatrix} \quad (3)$$

The matrix of elastic coefficients, \mathbf{E} can be written as and 8×8 matrix,

$$\mathbf{E} = \begin{bmatrix} \mathbf{E}_m & \mathbf{E}_{mf} \\ \mathbf{E}_{mf}^T & \mathbf{E}_f \end{bmatrix} \quad (4)$$

The definition of $\mathbf{E}_m, \mathbf{E}_f$ characterizing the membrane and flexural behavior, respectively, and that of \mathbf{E}_{mf} containing the membrane/flexural coupling are computed in terms of the lamina material properties and the laminate stacking sequence (LSS) as described by equation (6.16) in [32]. When the stress resultants are defined so that the equilibrium equations are satisfied with zero load, the following identity holds [33]

$$\int_{\Omega} \mathbf{t}^T \mathbf{D} \mathbf{d} \, d\Omega = \int_{\Gamma} \mathbf{t}^T \mathbf{N}^T \mathbf{d} \, d\Gamma = \int_{\Gamma} \mathbf{t}_m^T \mathbf{N}_m^T \mathbf{d}_m \, d\Gamma + \int_{\Gamma} \mathbf{t}_f^T \mathbf{N}_f^T \mathbf{d}_f \, d\Gamma \quad (5)$$

where \mathbf{N} is the matrix collecting the components of the unit outward normal to the contour Γ , that can be split into membrane \mathbf{N}_m and bending \mathbf{N}_f parts

$$\mathbf{N} = \begin{bmatrix} \mathbf{N}_m & \mathbf{0} \\ \mathbf{0} & \mathbf{N}_f \end{bmatrix} \quad (6)$$

2.1 Mixed finite element

Assuming a mixed interpolation for the stress resultants and displacements, a discrete expression for the Hellinger–Reissner mixed strain energy (1) can be evaluated. In general, the mixed interpolation can be written as

$$\mathbf{t} = \mathbf{B} \mathbf{t}_e, \quad \mathbf{d} = \mathbf{U} \mathbf{d}_e \quad (7)$$

where \mathbf{B} is the matrix collecting the assumed stress modes, \mathbf{t}_e is the vector of stress parameters, \mathbf{U} is the matrix of the displacement shape functions and \mathbf{d}_e is the vector of the displacement and rotation kinematical parameters. Substituting (7) into (1) and integrating on the element domain Ω_e leads to the evaluation of the element mixed energy

$$\Phi_e[\mathbf{t}_e, \mathbf{d}_e] = \mathbf{t}_e^T \mathbf{D}_e \mathbf{d}_e - \frac{1}{2} \mathbf{t}_e^T \mathbf{H}_e \mathbf{t}_e, \quad \begin{cases} \mathbf{D}_e = \int_{\Omega_e} \{\mathbf{B}^T \mathbf{D} \mathbf{U}\} \, d\Omega \\ \mathbf{H}_e = \int_{\Omega_e} \{\mathbf{B}^T \mathbf{E}^{-1} \mathbf{B}\} \, d\Omega \end{cases} \quad (8)$$

where \mathbf{D}_e and \mathbf{H}_e are the compatibility and flexibility matrices, respectively [21]. Obviously, when the stress resultants satisfy equilibrium equation with zero load, the compatibility matrix can be evaluated directly on the element contour Γ_e . Really, recalling (5), holds

$$\mathbf{D}_e = \int_{\Gamma_e} \mathbf{B}^T \mathbf{N}^T \mathbf{U} \, d\Gamma \quad (9)$$

allowing the definition of displacement interpolation along the contour only.

3 Geometrically nonlinear formulation

A linear finite element can be made geometrically nonlinear using corotational algebra to describe the rigid body motion [16]. Following the original proposal by Rankin et. al [34,35], this framework is still used [36–41]. With respect to the fixed frame $\{\mathbf{e}_1, \mathbf{e}_2, \mathbf{e}_3\}$, a corotational (CR) frame $\{\bar{\mathbf{e}}_1, \bar{\mathbf{e}}_2, \bar{\mathbf{e}}_3\}$ is defined as

$$\bar{\mathbf{e}}_k = \mathbf{Q}[\boldsymbol{\alpha}] \mathbf{e}_k, \quad k = 1..3 \quad (10)$$

with \mathbf{Q} being a rigid rotation, parametrized by the rotation vector $\boldsymbol{\alpha}$ according to Rodrigues' formulation [42] (see Fig. 1). The origin is assumed to be translated by vector \mathbf{c} . Denoting by \mathbf{d} and \mathbf{R} the displacement and the rotation associated to position \mathbf{X} in the fixed reference frame, the following geometrical relationships hold

$$\bar{\mathbf{d}} = \mathbf{Q}^T (\mathbf{X} + \mathbf{d} - \mathbf{c}) - \mathbf{X} \quad , \quad \bar{\mathbf{R}} = \mathbf{Q}^T \mathbf{R} \quad (11)$$

with $\bar{\mathbf{d}}$ and $\bar{\mathbf{R}}$ being the displacement and the rotation in the corotational frame. Using a vector parametrization for $\bar{\mathbf{R}}$ and \mathbf{R} and denoting by $\bar{\boldsymbol{\psi}}$ and $\boldsymbol{\psi}$ the rotation vectors, we have

$$\bar{\boldsymbol{\psi}} = \log(\bar{\mathbf{R}}[\bar{\boldsymbol{\psi}}]) = \log(\mathbf{Q}^T[\boldsymbol{\alpha}] \mathbf{R}[\boldsymbol{\psi}]) \quad (12)$$

A CR frame can be defined for each element through the element rotation vector $\boldsymbol{\alpha}_e$ which is a function of the element kinematical parameters \mathbf{d}_e in the fixed frame

$$\boldsymbol{\alpha}_e = \boldsymbol{\alpha}_e[\mathbf{d}_e] \quad (13)$$

The local kinematical parameters $\bar{\mathbf{d}}_e$ in the CR frame are related to \mathbf{d}_e by the geometrical transformation

$$\bar{\mathbf{d}}_e = \mathbf{g}[\mathbf{d}_e] \quad (14)$$

where \mathbf{g} collects the CR transformations for displacements (11) and rotations (12) opportunely rearranged once fixed the definition of local kinematical parameters $\bar{\mathbf{d}}_e$ of the finite element.

Based on the above relations, the linear finite element characterized by energy (8) can be transformed into a geometrically nonlinear element simply by introducing a corotational description and assuming that the element kinematical parameters in eq. (8) are referred to the corotational frame. This leads to:

$$\Phi_e[\mathbf{t}_e, \mathbf{d}_e] = \mathbf{t}_e^T \mathbf{D}_e \mathbf{g}[\mathbf{d}_e] - \frac{1}{2} \mathbf{t}_e^T \mathbf{H}_e \mathbf{t}_e \quad (15)$$

The element energy can be expressed in terms of the element vector

$$\mathbf{u}_e = \{\mathbf{t}_e, \mathbf{d}_e\}^T \quad (16)$$

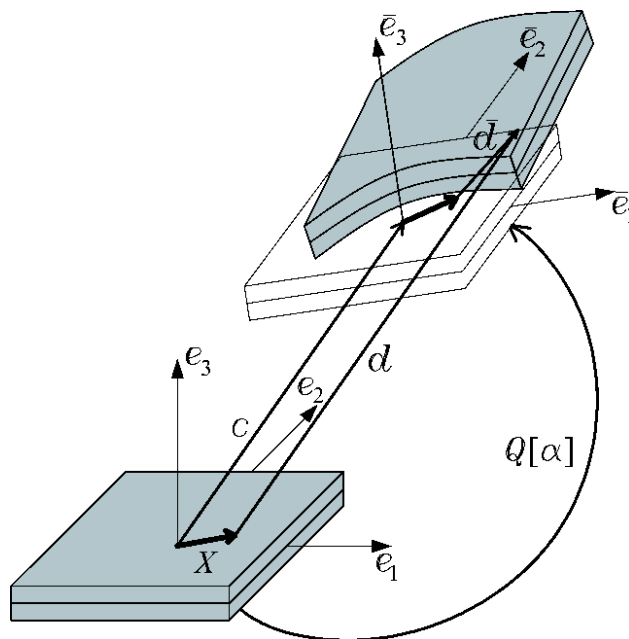


Figure 1: Corotational frame.

which collects all the parameters defining the element configuration in a single vector and can be related to the global configuration vector \mathbf{u} through the standard assemblage procedure

$$\mathbf{u}_e = \mathbf{A}_e \mathbf{u} \quad (17)$$

where the matrix \mathbf{A}_e implicitly contains the link constraints between elements. For the Hellinger-Reissner formulation used here, the components of \mathbf{u} are the global displacements/rotations of the nodes of the elements and the stress parameters of each element. Note that, the stress parameters can be solved at the element level, and then a pseudo-compatible scheme can be employed [43].

4 Flat linear finite element in corotational frame

The mixed isostatic self-equilibrated flat shell element MISS-4 [21] is used as the starting point here. It is a 4-node quadrilateral externally defined by 24 kinematical dofs and internally by an isostatic self-equilibrated stress expansion represented by 18 parameters.

The local reference frame is a Cartesian frame $\{\mathbf{e}_1, \mathbf{e}_2, \mathbf{e}_3\}$ defined so that the average Jacobian of the iso-parametric transformation is symmetric. For each side Γ_k , connecting nodes i and j in counterclockwise order, we define Ξ_k , Δ_k and its external normal \mathbf{n}_k according to the following expressions

$$\begin{aligned} \Xi_k &= \begin{bmatrix} \Xi_{kx} \\ \Xi_{ky} \end{bmatrix} = \begin{bmatrix} x_j + x_i \\ y_j + y_i \end{bmatrix} \\ \Delta_k &= \begin{bmatrix} \Delta_{kx} \\ \Delta_{ky} \end{bmatrix} = \begin{bmatrix} x_j - x_i \\ y_j - y_i \end{bmatrix} \\ \mathbf{n}_k &= \begin{bmatrix} n_{kx} \\ n_{ky} \end{bmatrix} = \frac{1}{L_k} \begin{bmatrix} \Delta_{ky} \\ -\Delta_{kx} \end{bmatrix} \end{aligned} \quad (18)$$

with $L_k = \sqrt{\Delta_{kx}^2 + \Delta_{ky}^2}$ being the side length. The one-dimensional abscissa $-1 \leq \zeta \leq 1$ along Γ_k is defined as

$$x = \frac{1}{2}(\Xi_{kx} + \Delta_{kx} \zeta) \quad , \quad y = \frac{1}{2}(\Xi_{ky} + \Delta_{ky} \zeta) \quad (19)$$

The membrane and bending stress modes are assumed to be uncoupled and the stress resultants approximation is written as

$$\begin{bmatrix} \mathbf{t}_m \\ \mathbf{t}_f \end{bmatrix} = \begin{bmatrix} \mathbf{B}_m & \mathbf{0} \\ \mathbf{0} & \mathbf{B}_f \end{bmatrix} \begin{bmatrix} \boldsymbol{\beta}_m \\ \boldsymbol{\beta}_f \end{bmatrix} \quad (20)$$

with $\mathbf{B}_m, \mathbf{B}_f$ are the matrices collecting the approximating functions for the membrane and flexural part, respectively, and $\boldsymbol{\beta}_m, \boldsymbol{\beta}_f$ are the corresponding stress parameters.

The membrane behavior of MISS-4 is represented by 9 stress parameters

$$\mathbf{B}_m = \begin{bmatrix} 1 & 0 & 0 & y & 0 & x & 0 & y^2 & -2a^2xy \\ 0 & 1 & 0 & 0 & x & 0 & y & -x^2 & 2b^2xy \\ 0 & 0 & 1 & 0 & 0 & -y & -x & 0 & a^2y^2 - b^2x^2 \end{bmatrix} \quad (21)$$

where a and b are the diagonal coefficients of the Jacobian matrix of the iso-parametric transformation [25].

The flexural stress resultants are described using 9 stress parameters

$$\mathbf{B}_f = \begin{bmatrix} 1 & 0 & 0 & x & 0 & y & 0 & xy & 0 \\ 0 & 1 & 0 & 0 & x & 0 & y & 0 & xy \\ 0 & 0 & 1 & 0 & y\bar{c} & x/\bar{c} & 0 & 0 & 0 \\ 0 & 0 & 0 & -1 & -\bar{c} & 0 & 0 & -y & 0 \\ 0 & 0 & 0 & 0 & 0 & -1/\bar{c} & -1 & 0 & -x \end{bmatrix} \quad (22)$$

where $\bar{c} = a^2/b^2$. The stress resultant approximation (20) is self-equilibrated and isostatic [43]. Really, the stress resultants interpolation is represented by 18 parameters corresponding to deformation modes of the elements (24 kinematical parameters minus 6 rigid body motion).

The interpolation of displacements and rotations is based on a 4-node element with 6 degrees of freedom (dof) per node. Recalling that the stress satisfies the equilibrium equation, the internal work can be obtained by integration along the element contour and, therefore, displacements and rotations need to be defined solely on the element boundary. The displacement interpolation along each side is defined as the sum of three terms as follows

$$\bar{\mathbf{d}}_k[\zeta] = \bar{\mathbf{d}}_{kl}[\zeta] + \bar{\mathbf{d}}_{kq}[\zeta] + \bar{\mathbf{d}}_{kc}[\zeta] \quad (23)$$

The first term is a linear expansion

$$\bar{\mathbf{d}}_{kl}[\zeta] = \frac{1}{2}[(1 - \zeta)\bar{\mathbf{d}}_e^{(i)} + (1 + \zeta)\bar{\mathbf{d}}_e^{(j)}] \quad \text{with} \quad \begin{cases} \bar{\mathbf{d}}_e^{(i)} = [\bar{d}_x^{(i)}, \bar{d}_y^{(i)}, \bar{d}_z^{(i)}]^T \\ \bar{\mathbf{d}}_e^{(j)} = [\bar{d}_x^{(j)}, \bar{d}_y^{(j)}, \bar{d}_z^{(j)}]^T \end{cases} \quad (24)$$

where i and j denote the nodes of side k . The second and third terms correspond to a quadratic and a cubic expansion for the normal component of the side displacement

$$\begin{cases} \bar{\mathbf{d}}_{kq}[\zeta] = \frac{1}{8} L_k (\zeta^2 - 1) \begin{bmatrix} (\bar{\varphi}_z^{(i)} - \bar{\varphi}_z^{(j)}) \mathbf{n}_k \\ -(\bar{\varphi}_e^{(i)} - \bar{\varphi}_e^{(j)})^T \mathbf{n}_k \end{bmatrix} \\ \bar{\mathbf{d}}_{kc}[\zeta] = \frac{1}{4} L_k \zeta (1 - \zeta^2) \begin{bmatrix} \mathbf{n}_k \\ 0 \end{bmatrix} \bar{\alpha} \end{cases} \quad \text{with} \quad \begin{cases} \bar{\varphi}_e^{(i)} = [\bar{\varphi}_x^{(i)}, \bar{\varphi}_y^{(i)}]^T \\ \bar{\varphi}_e^{(j)} = [\bar{\varphi}_x^{(j)}, \bar{\varphi}_y^{(j)}]^T \end{cases} \quad (25)$$

The parameter $\bar{\alpha}$ in the cubic term is taken as the average distortional in-plane nodal rotation

$$\bar{\alpha} = \frac{1}{4} \sum_{i=1}^4 \bar{\varphi}_z^{(i)} - \bar{\varphi}_{ze} \quad (26)$$

where $\bar{\varphi}_{ze}$ is the average in-plane rigid rotation of the element

$$\bar{\varphi}_{ze} = \mathbf{N}_\alpha \bar{\mathbf{d}}_{me}, \quad \mathbf{N}_\alpha = \frac{1}{4\Omega_e} [-\Delta_{4y}, \Delta_{4x}, -\Delta_{1y}, \Delta_{1x}, -\Delta_{2y}, \Delta_{2x}, -\Delta_{3y}, \Delta_{3x}] \quad (27)$$

where $\bar{\mathbf{d}}_{me}$ is 12-component vector collecting the kinematical parameters that represent the membrane behavior of the element, i.e., $\bar{d}_x^{(i)}$, $\bar{d}_y^{(i)}$, $\bar{\varphi}_z^{(i)}$.

Finally, a simple bilinear interpolation is assumed for bending rotations along the edge [33]

$$\bar{\varphi}_k[\zeta] = \frac{1}{2} [(1 - \zeta)\bar{\varphi}^{(i)} + (1 + \zeta)\bar{\varphi}^{(j)}] \quad (28)$$

The corotational frame is obtained by simply setting the rotation vector equal to the average nodal rotations in the fixed frame

$$\boldsymbol{\alpha}_e = \frac{1}{4} \sum_{i=1}^4 \boldsymbol{\varphi}_e^{(i)} \quad (29)$$

This choice offers a good compromise between accuracy and simplicity in the evaluation of high order energy variations for asymptotic analysis [16]. The choice (29) allows the geometrical transformation law to be defined as (14).

5 KOITER ASYMPTOTIC FINITE ELEMENT ANALYSIS

To apply the asymptotic approach to the corotational version of element MISS-4, explicit expressions for the second-, third- and fourth-order energy variations with respect to a configuration which can be either the initial or the bifurcation one, have to be computed [16], for both cases, updating the configuration, we can assume $\mathbf{d}_e = \mathbf{0}$.

The corotational approach is very convenient to express the strain energy variations, because the only nonlinearity is limited to the geometrical relationship $\mathbf{g}[\mathbf{d}_e]$, eq. (14). The Taylor expansion of this relationship can be written as

$$\mathbf{g}[\mathbf{d}_e] = \mathbf{g}_1[\mathbf{d}_e] + \frac{1}{2} \mathbf{g}_2[\mathbf{d}_e, \mathbf{d}_e] + \frac{1}{6} \mathbf{g}_3[\mathbf{d}_e, \mathbf{d}_e, \mathbf{d}_e] + \frac{1}{24} \mathbf{g}_4[\mathbf{d}_e, \mathbf{d}_e, \mathbf{d}_e, \mathbf{d}_e] + \dots \quad (30)$$

where \mathbf{g}_n are n -multilinear symmetric forms which express the n th Fréchet variations of function $\mathbf{g}[\mathbf{d}_e]$. In the following, vector \mathbf{u}_i ($i = 1 \dots 4$) denotes a generic variation of the global finite element configuration vector and vector $\mathbf{u}_{ei} = \mathbf{A}_e \mathbf{u}_i = \{\mathbf{t}_{ei}, \mathbf{d}_{ei}\}^T$ the corresponding vector at the element level, that collects stress and displacement parameters. With the same notation \mathbf{u}_0 and \mathbf{u}_{e0} are the global and element reference configuration vectors.

5.1 Second-order variations

Second-order energy variations are used in the evaluation of the fundamental mode and the buckling modes. In both cases, using expansion (30) and the energy expression (15), the contribution of the element to the energy variation can be expressed as

$$\Phi_e'' \mathbf{u}_{e1} \mathbf{u}_{e2} = \mathbf{t}_{e1}^T \mathbf{D}_e \mathbf{g}_1[\mathbf{d}_{e2}] + \mathbf{t}_{e2}^T \mathbf{D}_e \mathbf{g}_1[\mathbf{d}_{e1}] - \mathbf{t}_{e1}^T \mathbf{H}_e \mathbf{t}_{e2} + \mathbf{t}_{e0}^T \mathbf{D}_e \mathbf{g}_2[\mathbf{d}_{e1}, \mathbf{d}_{e2}] \quad (31)$$

Introducing matrices \mathbf{L}_1 and $\mathbf{G}[t_e]$ through the following equivalences

$$\mathbf{L}_1 \mathbf{d}_{ej} = \mathbf{g}_1[\mathbf{d}_{ej}] \quad , \quad \mathbf{d}_{e1}^T \mathbf{G}[t_{e0}] \mathbf{d}_{e2} = \mathbf{t}_{e0}^T \mathbf{D}_e \mathbf{g}_2[\mathbf{d}_{e1}, \mathbf{d}_{e2}], \quad (32)$$

eq. (31) can be rearranged in a more compact form:

$$\mathbf{u}_{e1}^T \Phi_e'' \mathbf{u}_{e2} = \mathbf{u}_{e1}^T \mathbf{K}_e \mathbf{u}_{e2} \quad , \quad \mathbf{K}_e = \begin{bmatrix} -\mathbf{H}_e & \mathbf{D}_e \mathbf{L}_1 \\ \mathbf{L}_1^T \mathbf{D}_e^T & \mathbf{G}[t_{e0}] \end{bmatrix} \quad (33)$$

The mixed tangent matrix of the element \mathbf{K}_e can be directly used, through a standard assemblage process, to obtain the overall stiffness matrix \mathbf{K}

$$\mathbf{u}_1^T \Phi'' \mathbf{u}_2 = \mathbf{u}_1^T \mathbf{K} \mathbf{u}_2 \quad , \quad \mathbf{K} = \sum_e \mathbf{A}_e^T \mathbf{K}_e \mathbf{A}_e \quad (34)$$

5.2 Third-order variations

Third-order energy variations are used in Koiter analysis to evaluate the third-order coefficients and are also used to evaluate the secondary force vectors. The element contribution to the scalar coefficients can be easily calculated using the general formula

$$\begin{aligned} \Phi_e''' \mathbf{u}_{e1} \mathbf{u}_{e2} \mathbf{u}_{e3} &= \mathbf{t}_{e1}^T \mathbf{D}_e \mathbf{g}_2[\mathbf{d}_{e2}, \mathbf{d}_{e3}] + \mathbf{t}_{e2}^T \mathbf{D}_e \mathbf{g}_2[\mathbf{d}_{e3}, \mathbf{d}_{e1}] + \mathbf{t}_{e3}^T \mathbf{D}_e \mathbf{g}_2[\mathbf{d}_{e1}, \mathbf{d}_{e2}] \\ &+ \mathbf{t}_{e0}^T \mathbf{D}_e \mathbf{g}_3[\mathbf{d}_{e1}, \mathbf{d}_{e2}, \mathbf{d}_{e3}] \end{aligned} \quad (35)$$

Then the element contributions can be simply added to get the global values. On the other hand, taking advantage of the above expression, the element contribution to vector secondary force vector can be evaluated by

$$\Phi_e''' \mathbf{u}_{e1} \mathbf{u}_{e2} = \mathbf{p}_e = \begin{bmatrix} \mathbf{D}_e \mathbf{g}_2[\mathbf{d}_{e1}, \mathbf{d}_{e2}] \\ \mathbf{G}[t_{e1}] \mathbf{d}_{e2} + \mathbf{G}[t_{e2}] \mathbf{d}_{e1} + \mathbf{q}[t_{e0}, \mathbf{d}_{e1}, \mathbf{d}_{e2}] \end{bmatrix} \quad (36)$$

where vector \mathbf{q} is defined according to the following condition:

$$\mathbf{d}_{e3}^T \mathbf{q}[t_{e0}, \mathbf{d}_{e1}, \mathbf{d}_{e2}] = \mathbf{t}_{e0}^T \mathbf{D}_e \mathbf{g}_3[\mathbf{d}_{e1}, \mathbf{d}_{e2}, \mathbf{d}_{e3}] \quad (37)$$

Then, the overall vector is then obtained by a standard assemblage

$$\Phi''' \mathbf{u}_1 \mathbf{u}_2 = \sum_e \mathbf{A}_e^T \mathbf{p}_e[\mathbf{u}_{e1}, \mathbf{u}_{e2}]$$

5.3 Fourth-order variations

Finally, fourth-order energy variations, used to evaluate the fourth-order coefficients, can be computed by summing the relevant element contributions based on the following expression

$$\begin{aligned} \Phi_e'''' \mathbf{u}_{e1} \mathbf{u}_{e2} \mathbf{u}_{e3} \mathbf{u}_{e4} &= \mathbf{t}_{e1}^T \mathbf{D}_e \mathbf{g}_3[\mathbf{d}_{e2}, \mathbf{d}_{e3}, \mathbf{d}_{e4}] + \mathbf{t}_{e2}^T \mathbf{D}_e \mathbf{g}_3[\mathbf{d}_{e3}, \mathbf{d}_{e4}, \mathbf{d}_{e1}] \\ &+ \mathbf{t}_{e3}^T \mathbf{D}_e \mathbf{g}_3[\mathbf{d}_{e4}, \mathbf{d}_{e1}, \mathbf{d}_{e2}] + \mathbf{t}_{e4}^T \mathbf{D}_e \mathbf{g}_3[\mathbf{d}_{e1}, \mathbf{d}_{e2}, \mathbf{d}_{e3}] \\ &+ \mathbf{t}_{e0}^T \mathbf{D}_e \mathbf{g}_4[\mathbf{d}_{e1}, \mathbf{d}_{e2}, \mathbf{d}_{e3}, \mathbf{d}_{e4}] \end{aligned} \quad (38)$$

6 NUMERICAL RESULTS

In the following, three benchmarks are analyzed. The first is a simply supported plate under uniaxial compression with different LSS [26]. The accuracy in the recovery critical and post-critical behavior are shown and the performance in terms of computational cost are compared with Riks path-following analysis. The second is a hinged cylindrical roof, that is a classical test [27] with a strong non linear precritical behavior and, as in the first benchmark, with a post-critical dominated by the first buckling mode. The last is a channel column, studied experimentally by [28] and aimed to show the accuracy and good performance in the analysis of folded plate including buckling mode interaction [44].

The accuracy and reliability of the results are closely related to the use of geometrically exact structural models and mixed formulation, the latter is necessary to prevent extrapolation locking phenomena [45]. The use of a corotational formulation coupled with a mixed finite element allows to easily satisfy previous requirements.

Moreover, Koiter approach being based on asymptotic expansion, allows to recover the equilibrium path in an approximate fashion. The best accuracy is available for the precritical and the initial post-critical behavior. A study of convergence can be found in [47], for the Koiter asymptotic approach called simple linear algorithm as proposed in [45] and very good results was proven. The currently used approach called full quadratic algorithm (see [10] and references therein) has shown better performance than simple linear one in all experiences done.

6.1 Square plate under compression

The buckling and post-buckling analysis of a laminated, simply-supported square plate under uniaxial membrane load [26] is presented and comparison with Riks path-following analysis using ABAQUS [48] is made. The lamina materials properties are $E_1 = 181$ GPa, $E_2 = 10.27$ GPa, $G_{12} = 7.17$ GPa, $\nu_{12} = 0.28$. The thickness is $t = 1.27210^{-4}$ m while the length is $l = 0.508$ m.

To evaluate accuracy, an test is performed for a simply supported $[0/90]_{4S}$ square plate ($h \times h$) subjected to uniaxial edge pressure λ . The critical loads are listed in Table 1 and the buckling modes are shown in Fig. 2. Note that h^2 convergence is achieved for critical values as shown in Fig. 3.

[0/90] _{4S}				
mesh	λ_1	λ_2	λ_3	λ_4
4x4	1.7562	5.0349	12.089	12.543
8x8	1.5472	4.0021	7.0816	9.0840
16x16	1.5002	3.7684	6.2008	8.1365
32x32	1.4892	3.7126	6.0054	7.9138
64x64	1.4867	3.6990	5.9588	7.8593
64x64 (S8R)	1.4861	3.6947	5.9443	7.8414

Table 1: Square plate under uniaxial compression. Convergence of buckling loads with mesh refinement.

Then, the accuracy of the post-critical behavior is investigated by looking at the convergence of the fourth order form \mathbb{B}_{ijhk} [10], which is reported in Fig. 3, showing convergence of order h^2 .

Then, the post-critical behavior for different LLS was calculated. The equilibrium paths graphed in Fig. 4 when compared with those obtained using path-following analysis confirm good accuracy

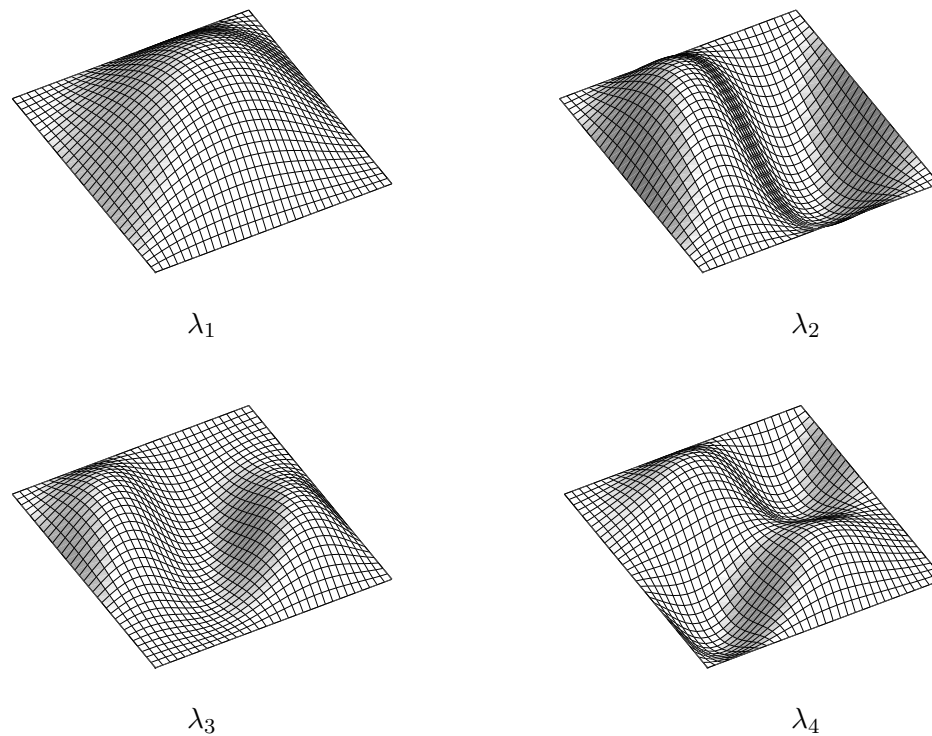


Figure 2: Square plate under uniaxial compression. Buckling modes corresponding to buckling loads $\lambda_1, \dots, \lambda_4$.

both the pre-critical and in the initial post-critical behavior. As expected (see Section 6), up to the initial post-critical range the two equilibrium paths coincide while over the accuracy gradually decrease.

Finally, to compare the performance of Koiter’s analysis with that of Riks path-following analysis, the computational cost of one analysis is reported. The aim is to evaluate the time needed for both analysis. For Koiter analysis, a 64x64 element mesh (about 25000 dofs) was employed to analyze only one imperfection. The most time is spent performing the linear analysis (see eq. 3 in [16]), the buckling (see eq. 4 in [16]) and to evaluate the post-critical energy variations (see eq. 8 in [16]). Just a little fraction of the time is spent to recover the equilibrium path (eq. 9 in [16]). Note that only the last step needs to be redone for analyzing a different imperfection. The total time spent for each problem was about 12 seconds, where less than a tenth of second was spent for recovering the equilibrium path.

The Riks analysis is performed using a coarser, 40x40 mesh of linear S4R elements (about 9600 dofs) in Abaqus. The analysis is particularly sensible to the Risk control settings, including the initial imperfection, which must be chosen by the analyst either in the load or in the initial geometry. For this comparison only, a geometrical imperfection in the form of the first buckling mode with the maximum magnitude displacement equal to 10^{-4} mm is used. The initial step length is assumed to be a tenth of the total arc length, and the later is assumed to be 1.0. The maximum incrementation is assumed to be 10. The other Riks control settings are left at their Abaqus default values. These control settings are optimized through a careful tuning for this particular test. Note that each new

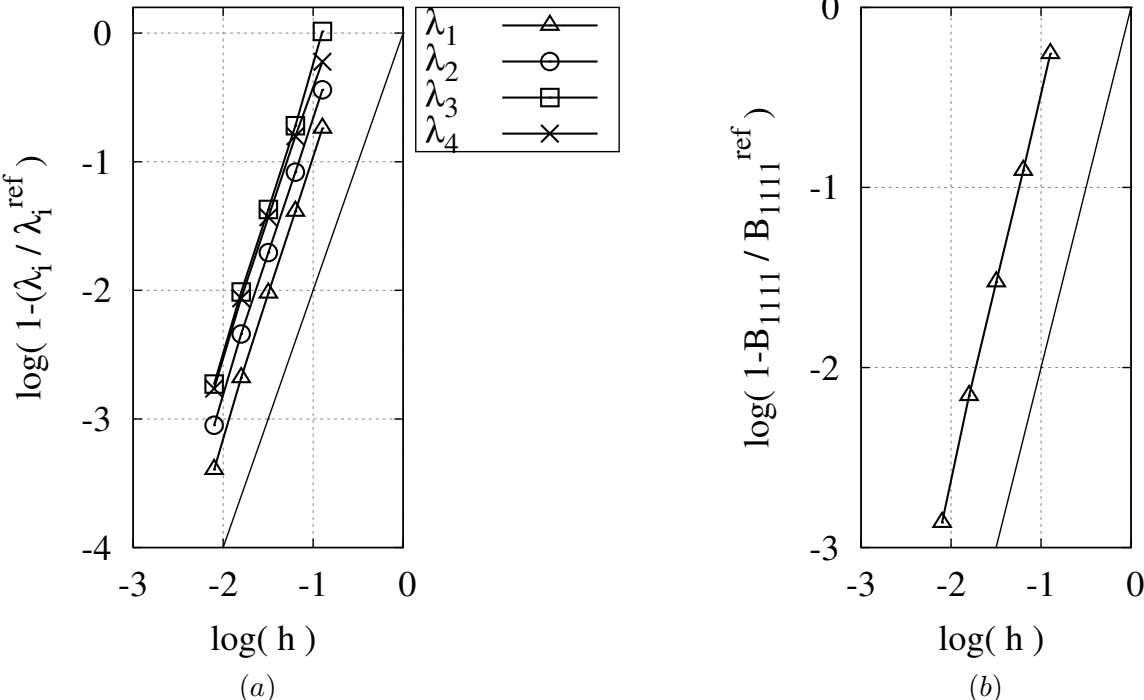


Figure 3: Square plate ($h \times h$) under uniaxial compression. (a) convergence of buckling loads and (b) convergence of post-critical quartic form. Solid line is for reference. On (a), ordinate is $\log |1 - \lambda_i / \lambda_i^{ref}|$. λ_i^{ref} calculated with a very fine mesh of Abaqus S8R elements. B_{1111}^{ref} calculated with a very fine mesh of MISS4 elements.

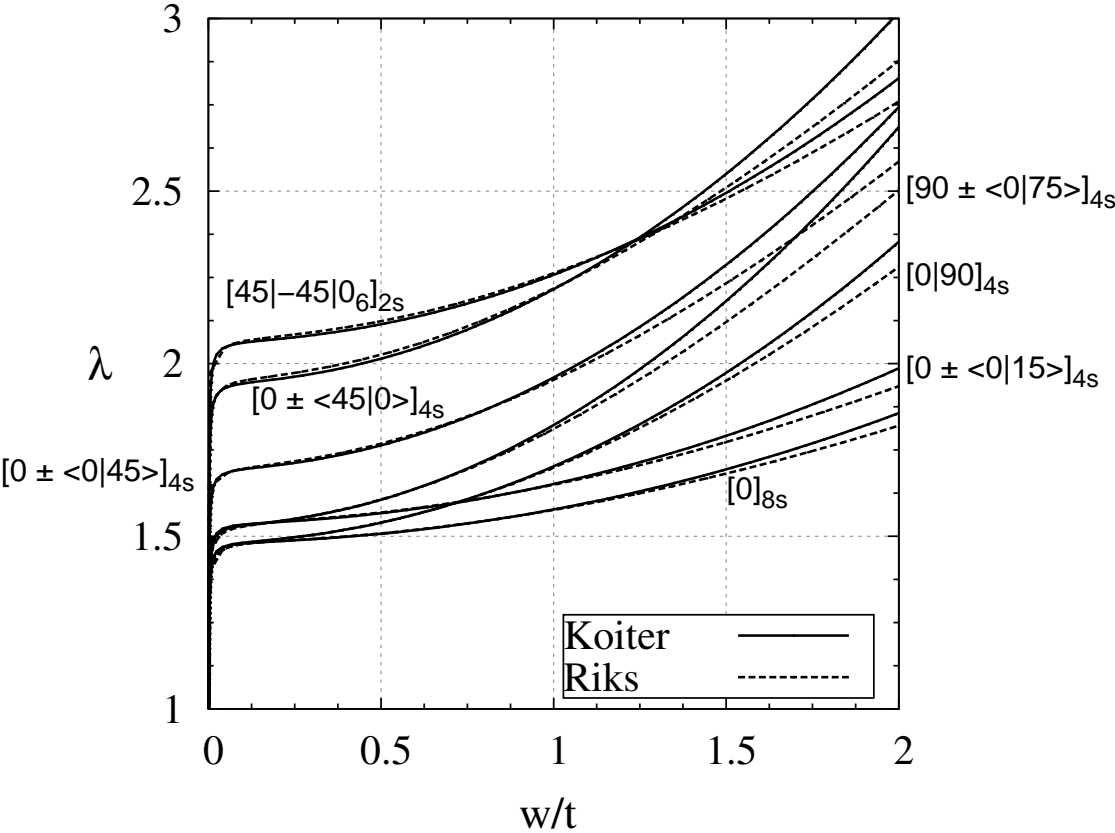


Figure 4: Square plate under compression. Equilibrium paths recovered using Koiter asymptotic analysis compared with that obtain Riks analysis. The load factor is indicated with λ while w denotes the transversal displacement of the center of the plate.

test needs news settings.

Each Riks analysis takes about 60 steps within a 1 or 2 equilibrium iterations, which impose matrix reforming, decomposition, and solving a linear system for each iteration. Note that the run must be fully redone for each new imperfection. The total time spent for one imperfection is reported in Table 2. The computations are performed on a Intel(R) Xeon(R) CPU E5-2620 2.00Ghz Dual Core, 32 GB Ram on a single core for both, Koiter and Riks analysis.

As shown in Table 2, the Koiter analysis is faster for every analysis. Obviously, Koiter's analysis becomes even more efficient when different imperfections are analyzed. When analyzing multiple imperfections, each imperfection requires the same time for Riks analysis, while the cost of Koiter's analysis becomes negligible because only the nonlinear system (see eq. 9 on [16]) needs to be solved.

problem	Koiter	Riks
1	11 s	39 s
2	14 s	38 s
3	13 s	54 s
4	13 s	37 s
5	11 s	36 s
6	13 s	58 s
7	13 s	44 s
Average	12.5 s	43.7 s

Table 2: Koiter's vs Riks analysis timing

6.2 Hinged cylindrical roof

The popular hinged cylindrical roof [27, 49] is analyzed in this section. The geometry, boundary condition and load are represented in Fig. 5. The length is $l = 2.54$ m, the radius is $R = 25.40$ m and the angle is $\beta = 0.1$ rad. The base load is $P = 10^3$ N.

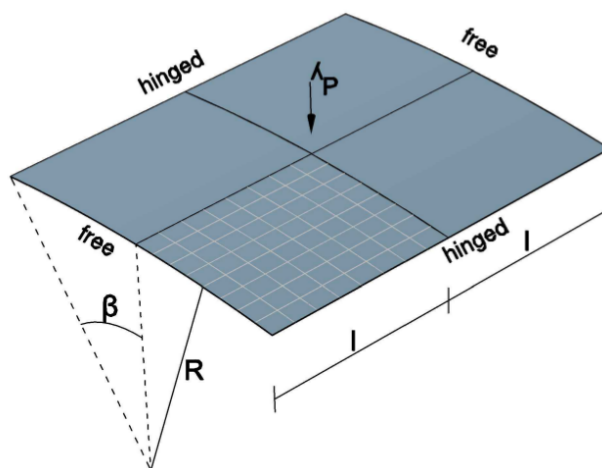


Figure 5: Hinged cylindrical roof. Geometry, boundary and load condition.

Three cases are considered. The first is a single layer with isotropic material and elastic modula

$E = 3102.75$ MPa, $\nu = 0.3$ and the thickness $t = 0.127$ m. The second and the third are laminated composite with LSS $[0/90/0]$ and $[90/0/90]$ respectively. The materials constants are $E_1 = 3300$ MPa, $E_2 = 1100$ Mpa, $G_{12} = 660$ Mpa, $\nu = 0.25$, and the thickness is $t = 0.127$ m. The interesting aspect of this test is the strong nonlinearity of the pre-critical path. The first buckling load is $\lambda_1 = 4.5607$ for isotropic single layer, $\lambda_1 = 3.5849$ and $\lambda_1 = 2.2177$ for LSS $[0/90/0]$ and $[90/0/90]$ respectively. The corresponding mode is represented in Fig. 6 for isotropic single layer.

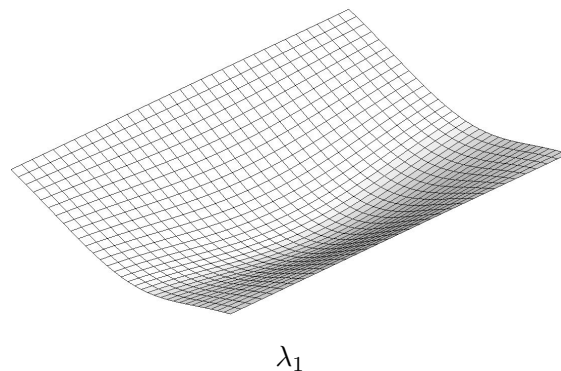


Figure 6: Hinged cylindrical roof. Buckling mode corresponding to buckling load λ_1 .

The equilibrium path recovered for laminated composite and for isotropic material are reported in Fig 7 in comparison with Riks analysis. Note that the limit load is about one-half of the value of the first buckling load, for all cases.

The good representation of pre-critical behavior, limit load, and initial post-critical path is clear also in Fig. 7 for this particularly difficult case. Really, the Koiter equilibrium path coincide with that of Riks analysis up to the limit point. The expected accuracy is shown while over the limit point the accuracy gradually decrease.

6.3 Channel section under compression

A channel section under compression is analyzed next. Experimental results for this problem are available in [28], being one of their more recent results in this field [50–52]. The geometry, load, and boundary conditions, as well as the LSS for each panel of the channel section are reported in Fig. 8.

The material data are $E_1 = 130.71$ GPa, $E_2 = 6.36$ GPa, $G_{12} = 4.18$ GPa, $\nu = 0.32$. The results of buckling analysis are reported in Fig. 9 for the six lower buckling modes. The analysis is performed with a fine mesh (16 elements on the wings, 32 on the web, and 120 along the height). Mode deflections involve both the wings and the web. Moreover, some of the critical loads are very close.

The equilibrium paths are reported in Fig. 10. Koiter's analysis is performed with a rough mesh (8 element on the wings, 16 on the web, and 60 along the height). The first six modes are reported. Two displacements components are plotted: the axial displacement u (mm) of the end section and the transversal displacement w (mm) at a quarter of the height in the center of the web. The equilibrium path recovered with Koiter's analysis is compared with Rik's path-following analysis. The results clearly show the accuracy in the recovery the initial post-critical behavior.

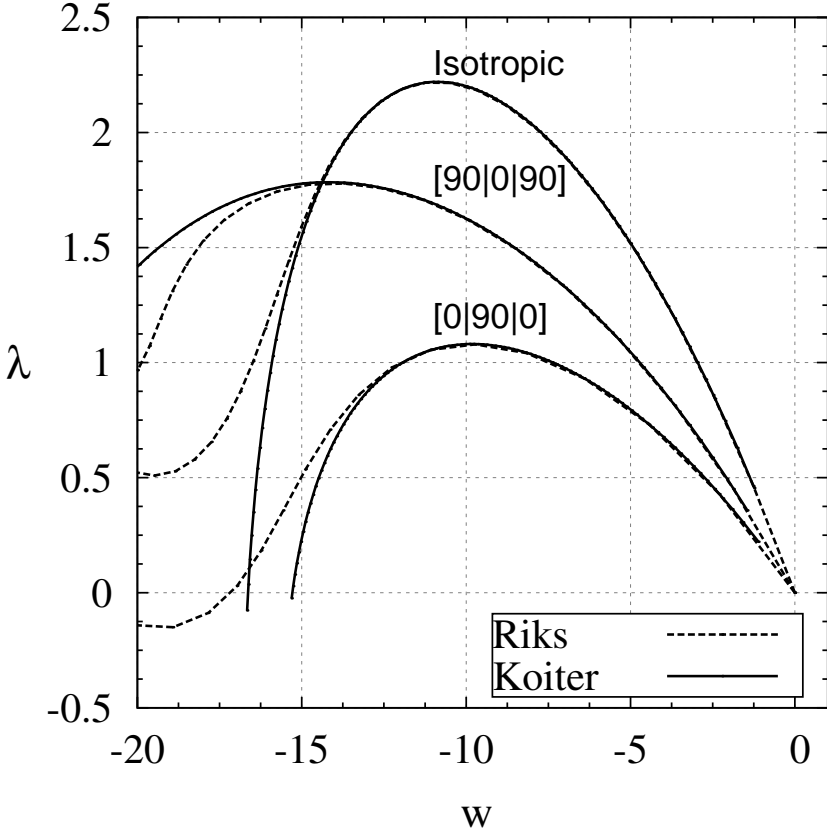


Figure 7: Hinged cylindrical roofs. Equilibrium paths. The load factor is indicated with λ while w (mm) denotes the transversal displacement of the center of the cylindrical roofs.

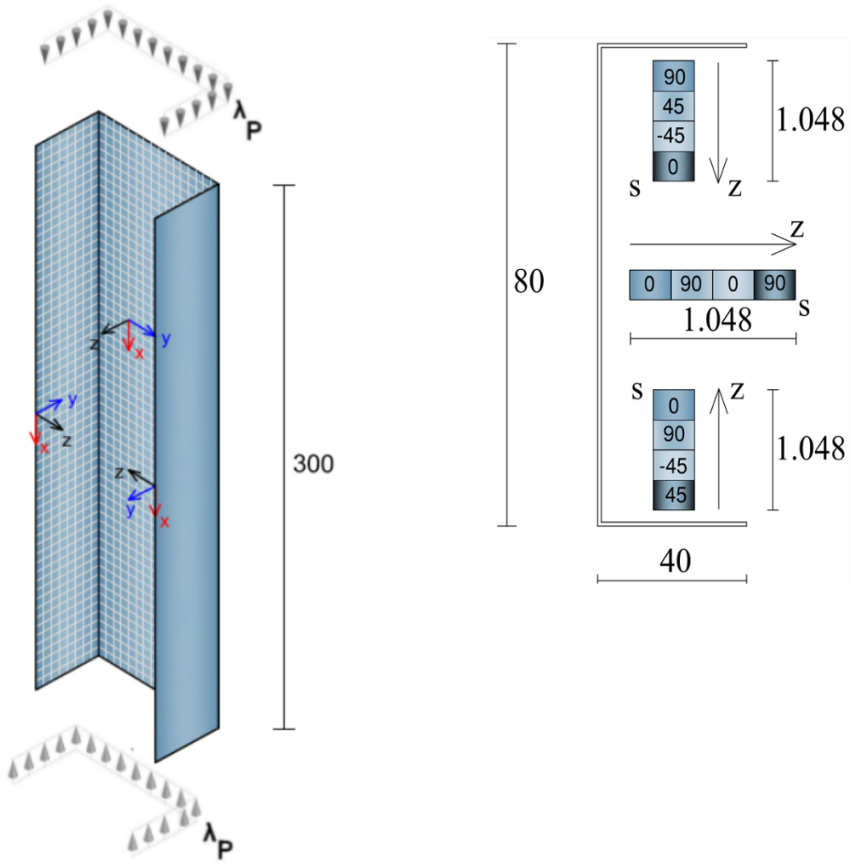


Figure 8: Channel section. Geometry, boundary, and load conditions. Dimensions are expressed in mm.

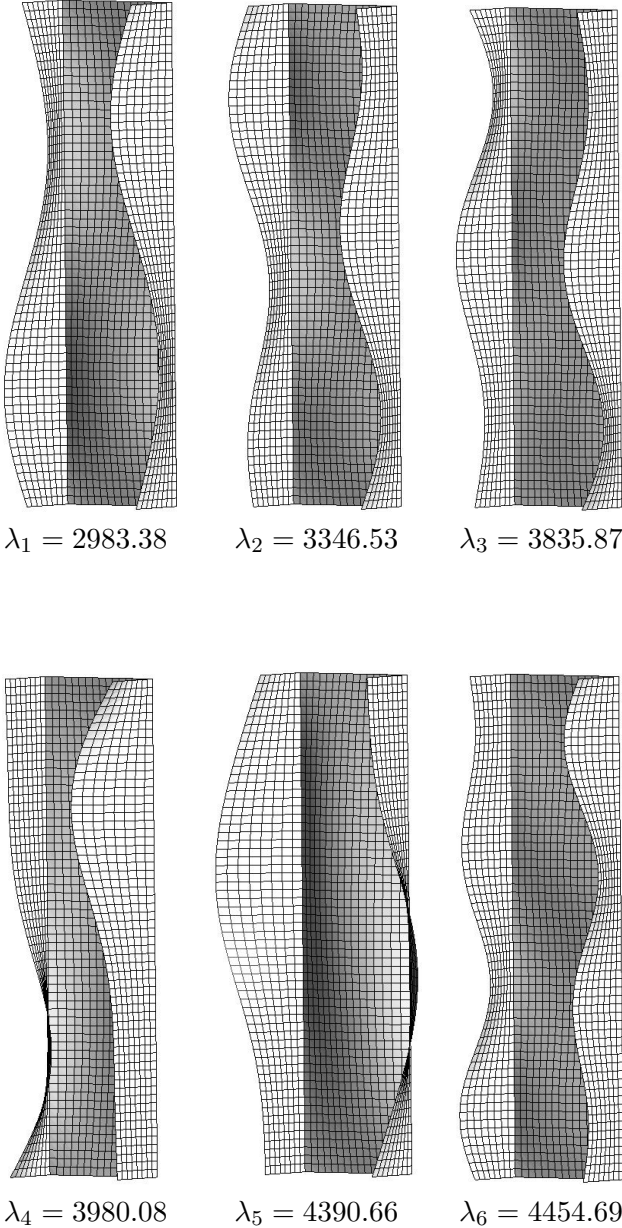


Figure 9: Channel section. Buckling modes corresponding to buckling loads $\lambda_1, \lambda_2, \dots, \lambda_6$.

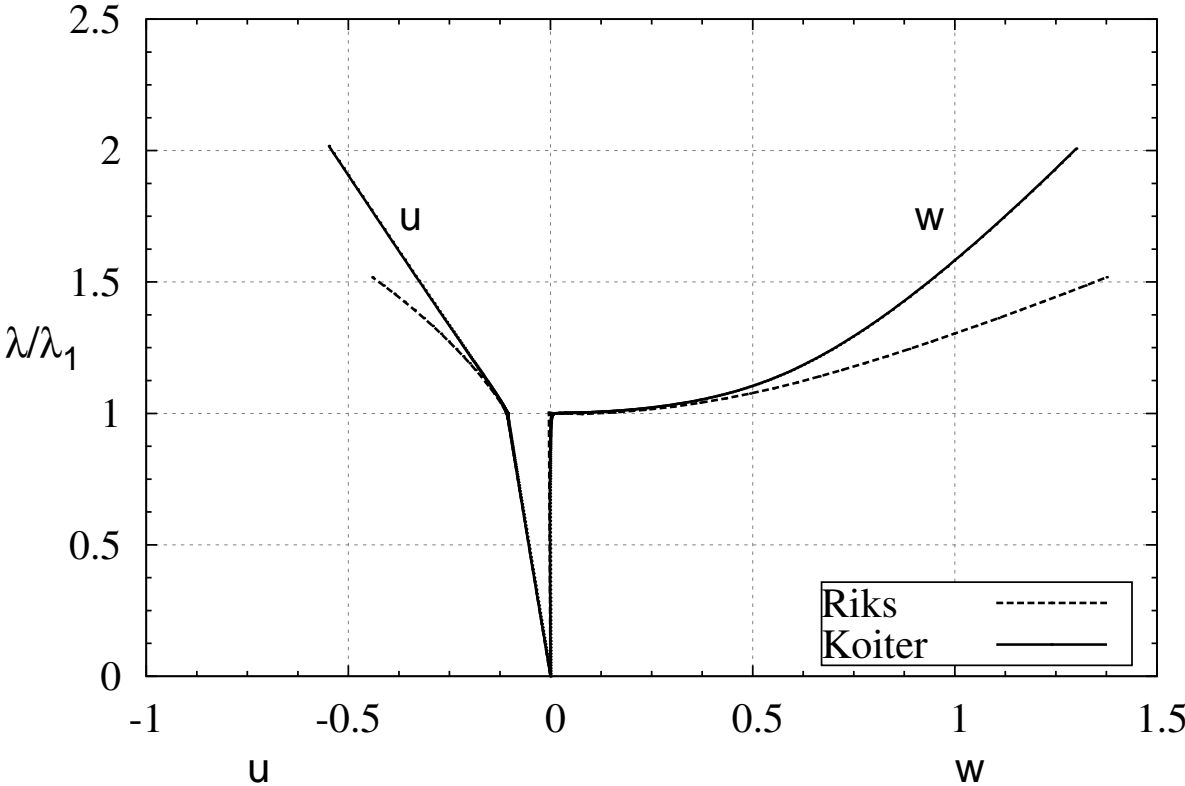


Figure 10: Channel section. Equilibrium paths recovered using Koiter asymptotic analysis compared with that obtain Riks analysis. Load factor is indicated with λ and it is normalized on the first buckling load λ_1 . In the abscissa are plotted the axial displacement u of the end section and the transversal displacement w at a quarter of the height in the center of the web.

7 Conclusions

Koiter's asymptotic analysis represents a valid, less computational expensive alternative to Riks path-following analysis for the recovery the initial post-critical behavior of composite structures, even those displaying strong pre-critical behavior and buckling mode interaction. Its use in the context of laminated composite folded plate (shell) structures has been demonstrated. The accuracy of the proposed element has been checked and the convergence of the critical and post-critical quantities show good performance, which can be attributed to the simplicity of the linear finite element employed and the choice of corotational formulation for the extension to nonlinear analysis of folded laminated composites. The computational cost has been monitored and the results show the advantage of Koiter's analysis versus Riks analysis, including considerations of accuracy and robustness for difficult test cases.

8 Acknowledgements

The first author acknowledges the support of the Energy Materials Science and Engineering (EMSE) program at West Virginia University. The remaining authors wish to acknowledge the RISPEISE cooperation project for their financial support.

References

- [1] Barbero EJ, DeVivo L. Beam-column design equations for wide-flange pultruded structural shapes. *J Compos Construction* 3(4):185–191, 1999.
- [2] Marín L, Trias D, Badalló P, Rus G, Mayugo JA. Optimization of Composite Stiffened Panels Under Mechanical and Hygrothermal Loads using Neural Networks and Genetic Algorithms. *Compos Struct* 2012; 94:3321–3326.
- [3] Collier C, Yarrington P. Composite grid-stiffened panel design for post buckling using hyper-sizer. AIAA-2002-1222, Denver Colorado 2002: 1–9.
- [4] Riks E. An incremental approach to the solution of snapping and buckling problems. *Int J Solids Struct* 1979;15:529–551.
- [5] Koiter WT. On the stability of elastic equilibrium. Ph.D. Thesis, University of Delft 1945. English Translation issued as NASA TT-F10 1967; 883 and AFFDL Report 1970; 70–25.
- [6] Flores FG, Godoy LA. Elastic postbuckling analysis via finite element and perturbation techniques. Part 1. Formulation *Int J Numer Methods Eng* 1992;33:1775–1794.
- [7] Pacoste C, Eriksson A. Element behavior in post-critical plane frame analysis. *Comput Meth Appl Mech Eng* 1995;125(1–4): 319–343.
- [8] Poulsen PN, Damkilde L. Direct determination of asymptotic structural postbuckling behaviour by the finite element method. *Int J Numer Methods Eng* 1998;42(4):685–702.
- [9] Abichou H, Zahrouni H, Potier-Ferry M. Asymptotic numerical method for problems coupling several nonlinearities. *Comput Meth Appl Mech Eng* 2002;191(51–52):5795–5810.

- [10] Casciaro R. Computational asymptotic post-buckling analysis of slender elastic structures. In: Pignataro, M., Gioncu, V. (Eds.), *Phenomenological and Mathematical Modeling in Structural Instabilities*. Springer Verlag 2005.
- [11] Rahman T, Jansen EL. Finite element based coupled mode initial post-buckling analysis of a composite cylindrical shell. *Thin Walled Struct* 2010;48(1):25–32.
- [12] Liang K, Abdalla M, Gurdal Z. A Koiter-Newton approach for nonlinear structural analysis. *Int J Numer Methods Eng* 2013; doi: 10.1002/nme.4581.
- [13] Rizzi N, Varano V, Gabriele S. Initial postbuckling behavior of thin-walled frames under mode interaction. *Thin Walled Struct* 2013;68:124–134.
- [14] Garcea G, Bilotta A, Madeo A, Casciaro R. *Direct Evaluation of the Post-Buckling Behavior of Slender Structures Through a Numerical Asymptotic Formulation, Direct Methods for Limit States in Structures and Materials*. Springer Netherlands 2014.
- [15] Raftoyiannis I, Godoy LA, Barbero EJ. Buckling mode interaction in composite plate assemblies. *Appl Mech Rev* 1995; 48(11/2):52–60.
- [16] Garcea G, Madeo A, Zagari G, Casciaro R. Asymptotic post-buckling FEM analysis using corotational formulation. *Int J Solids Struct* 2009; 6:377–397.
- [17] Garcea G, Madeo A, Casciaro R. The implicit corotational method and its use in the derivation of nonlinear structural models for beams and plates. *J Mech Mater Struct* 2012; 7(6):509–538.
- [18] Garcea G, Madeo A, Casciaro R. Nonlinear FEM analysis for beams and plate assemblages based on the implicit corotational method. *J Mech Mater Struct* 2012;7 (6):539–574.
- [19] Reddy JN. *Mechanics of Laminated Composite Plates and Shells - Theory and Analysis*, CRC Press Second Edition 2004.
- [20] Zinno R, Barbero EJ. Total Lagrangian formulation for laminated composite plates analysed by three-dimensional finite elements with two-dimensional kinematic constraints. *Comput Struct* 1995; 57(3): 455-466.
- [21] Madeo A, Zagari G, Casciaro R, de Miranda S. A mixed 4-node 3D plate element based on self-equilibrated isostatic stresses. Accepted for publication *IJSSD* 2013.
- [22] Zagari G, Madeo A, Casciaro R, de Miranda S, Ubertini F. Koiter analysis of folded structures using a corotational approach. *Int J Solids Struct* 2013; 50(1):755–765.
- [23] Allman DJ. A compatible triangular element including vertex rotations for plane elasticity analysis. *Comput Struct* 1984; 19(1-2):1–8.
- [24] Allman DJ. A quadrilateral finite element including vertex rotations for plane elasticity analysis. *Int J Numer Methods Eng* 1988;26(3):717–730.
- [25] Madeo A, Zagari G, Casciaro R. An isostatic quadrilateral membrane finite element with drilling rotations and no spurious modes. *Finite Elem Anal Des* 2011;50:21–32.
- [26] Raju G, Wu Z, Weaver PM. Postbuckling analysis of variable angle tow plates using differential quadrature method. *Compos Struct* 2013;106:74–84.

- [27] Sze KY, Liu XH, Lo SH. Popular benchmark problems for geometric nonlinear analysis of shells. *Finite Elem Anal Des* 2004;40: 1551–1569.
- [28] Debski H, Kubiak T, Teter A. Experimental investigation of channel-section composite profiles behavior with various sequences of plies subjected to static compression. *Thin Walled Struct* 2013;71:147–154.
- [29] Godoy LA, Barbero EJ, Raftoyiannis IG. Finite elements for post-buckling analysis. I - the w-formulation. *Comput Struct* 1995; 56(6):1009–1017.
- [30] Barbero EJ, Raftoyiannis IG, Godoy LA. Finite elements for post-buckling analysis. II - application to composite plate assemblies. *Comput Struct* 1995;56(6):1019–1028.
- [31] Barbero EJ. Prediction of buckling-mode interaction in composite columns. *Mech Compos Mater Struct* 2000;7(3):269–284.
- [32] Barbero EJ. *Introduction to Composite Materials Design-Second Edition*, CRC Press, Boca Raton, FL 2010.
- [33] de Miranda S, Ubertini F. A simple hybrid stress element for shear deformable plates. *Int J Numer Methods Eng* 2006; 65:808–833.
- [34] Rankin CC, Nour-Omid B. The use of projectors to improve finite element performance. *Comput Struct* 1988;30:257–267.
- [35] Nour-Omid B, Rankin CC. Finite rotation analysis and consistent linearization using projectors. *Comput Meth Appl Mech Eng* 1991;93:353–384.
- [36] Mostafa M, Sivaselvan MV, Felippa CA. A solid-shell corotational element based on ANDES, ANS and EAS for geometrically nonlinear structural analysis. *Int J Numer Methods Eng* 2013;95(2);145–180.
- [37] Mostafa M, Sivaselvan MV, Felippa CA. Reusing linear finite elements in material and geometrically nonlinear analysis-Application to plane stress problems, *Finite Elem Anal Des* 2013;69:62–72.
- [38] Caselli F, Bisegna P. Polar decomposition based corotational framework for triangular shell elements with distributed loads. *Int J Numer Methods Eng* 2013;95(6):499–528.
- [39] Li ZX, Liu YF, Izzuddin BA, Vu-Quoc L. A stabilized co-rotational curved quadrilateral composite shell element. *Int J Numer Methods Eng* 2011;86(8):975–999.
- [40] Li ZX, Zhou X, Vu-Quoc L, Izzuddin BA, Wei HY. A four-node corotational quadrilateral elastoplastic shell element using vectorial rotational variables. *Int J Numer Methods Eng* 2013;95:181–211.
- [41] Norachan P, Suthasupradit S, Kim KD. A co-rotational 8-node degenerated thin-walled element with assumed natural strain and enhanced assumed strain. *Finite Elem Anal Des* 2012;50:70–85.
- [42] Rodrigues O. Des lois géométriques qui régissent les déplacements d'un système solide dans l'espace, et de la variation des coordonnées provenant de ces déplacements considérés indépendamment des causes qui peuvent les produire. *Journal de Mathématiques Pures et Appliquées* 1840;5:380–440.

- [43] Bilotta A, Casciaro R. Assumed stress formulation of high order quadrilateral elements with an improved in-plane bending behaviour. *Comput Meth Appl Mech Eng* 2002;191(15-16):1523–1540.
- [44] Barbero EJ, Dede EK, Jones S. Experimental verification of buckling-mode interaction in intermediate-length composite columns. *Int J Solids Struct* 2000;37(29):3919–3934.
- [45] Garcea G, Salerno G, Casciaro R. Extrapolation locking and its sanitization in Koiter’s asymptotic analysis. *Comput Meth Appl Mech Eng* 1999;180(1-2):137–167.
- [46] Casciaro R, Salerno G, Lanzo AD. Finite element asymptotic analysis of slender elastic structures: A simple approach. *Int J Numer Methods Eng* 1992;35(7):1397–1426.
- [47] Brezzi F, Cornalba M, Di Carlo A. How to get around a simple quadratic fold. *Numerische Mathematik* 1986;48(4):417–427.
- [48] Hibbitt, Karlsson, Sorensen. *Abaqus theory manual*, version 6.8, Dassault 2009.
- [49] Andrade LG, Awruch AM, Morsch IB. Geometrically nonlinear analysis of laminate composite plates and shells using the eight-node hexahedral element with one-point integration. *Compos Struct* 2007;79:571–580.
- [50] Debski H, Kubiak T, Teter A. Buckling and postbuckling behaviour of thin-walled composite channel section column. *Compos Struct* 2013;100:195–204.
- [51] Teter A, Kolakowski Z. Interactive buckling and load carrying capacity of thin walled beam columns with intermediate stiffeners. *Thin Walled Struct* 2004;42:211–254.
- [52] Teter A, Kolakowski Z. Buckling of thin-walled composite structures with intermediate stiffeners. *Compos Struct* 2005;69: 421–428.